AIP | The Journal of Chemical Physics

Theoretical studies of He(1 S)+CH(X 2Π). II. Fully ab initio cross sections for the inelastic scattering and comparison with experiment

Millard H. Alexander, William R. Kearney, and Albert F. Wagner

Citation: The Journal of Chemical Physics **100**, 1338 (1994); doi: 10.1063/1.466611
View online: http://dx.doi.org/10.1063/1.466611
View Table of Contents: http://scitation.aip.org/content/aip/journal/jcp/100/2?ver=pdfcov
Published by the AIP Publishing

Articles you may be interested in

Ab initio study of the He(1 S)+CH(X 2Π) interaction
J. Chem. Phys. **105**, 9525 (1996); 10.1063/1.472820

Theoretical studies of He(1 S)+CH(X 2Π). I. Ab initio potential energy surfaces
J. Chem. Phys. **100**, 1326 (1994); 10.1063/1.466610

Differential and integral cross sections for the inelastic scattering of NO (X 2Π) by Ar based on a new ab initio potential energy surface
J. Chem. Phys. **99**, 7725 (1993); 10.1063/1.465702

A crossedbeam study of the stateresolved integral cross sections for the inelastic scattering of OH(X 2Π) with CO and N2
J. Chem. Phys. **94**, 6508 (1991); 10.1063/1.460279

Statetostate integral cross sections for the inelastic scattering of CH(X 2Π)+He: Rotational rainbow and orbital alignment
J. Chem. Phys. **91**, 821 (1989); 10.1063/1.457134

This article is copyrighted as indicated in the article. Reuse of AIP content is subject to the terms at: http://scitation.aip.org/termsconditions. Downloaded to IP: 141.209.100.60 On: Mon, 22 Dec 2014 16:43:09

Theoretical studies of He(^1S)+CH($X\ ^2\Pi$). II. Fully *ab initio* cross sections for the inelastic scattering and comparison with experiment

Millard H. Alexander and William R. Kearney[a)]
Department of Chemistry and Biochemistry, University of Maryland, College Park, Maryland 20742

Albert F. Wagner
Chemistry Division, Argonne National Laboratory, Argonne, Illinois 60439

(Received 23 October 1992; accepted 15 June 1993)

We report a series of full close-coupling calculations of integral cross sections for fine structure resolved, rotationally inelastic transitions of CH induced by collisions with He. These calculations use the necessary two CH($X\ ^2\Pi$)+He potential energy surfaces as determined by a variety of *ab initio* techniques described in the preceeding paper. The calculated $N=1\rightarrow N=2-7$ cross sections confirm a previous prediction of preferential population of final state levels in which the electronic wave function of the CH molecule is *antisymmetric* with respect to reflection in the plane of rotation of the molecule. A generally good overall agreement is found between the energy-dependent cross sections determined in earlier experiments of Macdonald and Liu and appropriate averages of the calculated cross sections. However, small, systematic, qualitative discrepancies persist between theory and experiment. Diagnostic calculations were carried out to identify the cause of these discrepancies. These calculations explored the influence of restrictions in basis set, configuration interaction, and functional forms used in fitting the potential energy surfaces. They also explored the consequences of the dynamical approximations of CH as a rigid rotor and the independence of the CH spin–orbit constant on the approach of the He partner. All these diagnostic calculations generally confirm the anticipated marginal influence of these approximations.

I. INTRODUCTION

In recent years there have been a considerable number of theoretical studies devoted to gas-phase, inelastic collisions of molecules in $^2\Pi$ electronic states. Inspired by concurrent experimental work,[1] several formal papers[2,3] set the framework for a number of applications to collisions involving the following molecules: CaF($A\ ^2\Pi$),[4] OH($X\ ^2\Pi$),[5–11] NO($X\ ^2\Pi$),[12–16] CN($X\ ^2\Sigma^+$,$A\ ^2\Pi$).[15] From this body of work, considerable insight into the dynamics of such inelastic collisions, for example, the origin of spin state and Λ doublet propensities, has been obtained. A qualitative analysis,[16] based on first-order perturbation theory, was shown to be useful in predicting which transitions between specific initial and final Λ doublet levels would be favored in collisions of $^2\Pi$ molecules which follow Hund's case (b), or intermediate case, coupling. One expects[16] to see propensities toward population of either symmetric [$\Pi(A')$][17] or antisymmetric [$\Pi(A'')$] Λ doublet levels, *regardless* of the initial Λ doublet level. These propensities arise from quantum mechanical interference, reflecting the fact that two potential energy surfaces are required to describe the interaction between a molecule in a Π electronic state and a closed shell partner.[3]

Over the past several years Liu and Macdonald have reported[18,19] an extensive series of crossed-beam experiments on the inelastic scattering of the CH radical in its ground $X\ ^2\Pi$ electronic state with atomic He. A rich set of information was obtained on the velocity dependence of cross sections for transitions into a number of Λ doublet, spin–orbit, and rovibrational states in this system. Because of this experimental interest, collisions of CH($X\ ^2\Pi$) with He can serve as a prototype for inelastic collisions of hydrides in $^2\Pi$ electronic states.[1] In a more specific sense, CH+He is the nonreactive analog of CH+D_2, also studied by Liu and Macdonald.[20] The dynamics calculations reported here are a prelude to more demanding calculations that can be performed on the family of potential energy surfaces for CH_3.

We report here integral cross sections for the CH($X\ ^2\Pi$)+He system, based on the potential energy surfaces determined by Kok, Wagner, and Dunning,[21] as described in the preceding paper (hereafter denoted as Paper I). These cross sections are then compared with the experimental results of Macdonald and Liu.[18,19] In addition, Paper I reports a variety of potential energy surfaces based on choices of basis set, the degree of configuration interaction, and the flexibility of the functional form used to fit the surface. The present article will explore the dynamical consequences of the variations in these surfaces.

The organization of this paper is as follows: In the next section we give a brief review of the relevant features of the quantum formulation of the scattering of a molecule in a $^2\Pi$ electronic state. Section III summarizes the scattering calculations which were performed. The behavior of the calculated integral cross sections are discussed in Sec. IV, and then compared with experiment in Sec. V. Section VI contains a study of the sensitivity of the calculated cross sections on the remaining dynamical approximations. A brief conclusion follows.

[a)]Present address: Department of Chemistry, University of Iowa, Iowa City, IO 55242.

 0021-9606/94/100(2)/1338/12/$6.00 © 1994 American Institute of Physics

This article is copyrighted as indicated in the article. Reuse of AIP content is subject to the terms at: http://scitation.aip.org/termsconditions. Downloaded to IP: 141.209.100.60 On: Mon, 22 Dec 2014 16:43:09

II. FORMAL ANALYSIS OF $^2\Pi$ SCATTERING

The total Hamiltonian for the collision of a diatomic molecule with a structureless atom can be written as

$$H(r,R,\theta,\mathbf{q}) = -\frac{\hbar^2}{2\mu R^2}\frac{\partial}{\partial R}R^2\frac{\partial}{\partial R}+\frac{\mathbf{l}^2}{2\mu R^2}+H_{\rm mol}(r,\mathbf{q}) + V(r,R,\theta,\mathbf{q}). \quad (1)$$

Here the usual Jacobi coordinates are r, the molecular internuclear separation; R, the separation between the centers of mass of the collision partners; and θ, the angle between the diatomic axis and the body-frame z axis. Also $\mathbf{q}$ designates, collectively, the electronic coordinates, μ denotes the collision reduced mass of the atom+diatomic system, and $\mathbf{l}$ designates the operator for the orbital angular momentum of the molecule with respect to the atom, with

$$\mathbf{l}^2=(J-\mathbf{J})^2. \quad (2)$$

Here J and $\mathbf{J}$ denote the operators for the total angular momentum of the triatomic system and the total angular momentum of the diatomic, respectively.

The internal Hamiltonian for the diatomic molecule, $H_{\rm mol}(r,\mathbf{q})$ in Eq. (1), can be written as

$$H_{\rm mol}(r,\mathbf{q}) = -\frac{\hbar^2}{2mr^2}\frac{\partial}{\partial r}r^2\frac{\partial}{\partial r}+\frac{(\mathbf{J}-\mathbf{L}-\mathbf{S})^2}{2mr^2}+H_{\rm so}(\mathbf{q};r) + H_{\rm el}(\mathbf{q};r). \quad (3)$$

Here m is the reduced mass of the diatomic, $\mathbf{L}$ and $\mathbf{S}$ designate the orbital and spin angular momentum of the electrons ($S=1/2$ and $L=1$ for a $^2\Pi$ molecule), $H_{\rm so}(\mathbf{q};r)$ is the spin–orbit operator, and $H_{\rm el}(\mathbf{q};r)$ is the usual Born–Oppenheimer electronic Hamiltonian.

In the quantum close-coupled treatment of the scattering, it is most convenient to expand the total wave function as a sum of products of wave functions which are eigenfunctions of the molecular Hamiltonian multiplied by functions which describe the orbital motion of the noble gas collision partner with respect to the diatomic molecule. The molecular wave functions are first written in an unsymmetrized (definite Λ) Hund's case (a) basis as[22–24]

$$|JM\Omega\Lambda S\Sigma\rangle = |JM\Omega\rangle\,|\Lambda S\Sigma\rangle, \quad (4)$$

where M and Ω denote the projections along, respectively, the space- and molecule-fixed z axes of $\mathbf{J}$, and Σ and Λ designate, respectively, the projections along the molecule-fixed z axis of $\mathbf{S}$ and $\mathbf{L}$. In Eq. (4) $|\Lambda S\Sigma\rangle$ and $|JM\Omega\rangle$ represent, respectively, the electronic and rotational parts of the wave function. Definite-parity combinations of these primitive wave functions are used as basis functions for diagonalizing the molecular Hamiltonian[22–24]

$$|JM\Omega\varepsilon\rangle = 2^{-1/2}[\,|JM\Omega\rangle\,|\Lambda S\Sigma\rangle+\varepsilon|JM\Omega\rangle\,|-\Lambda S-\Sigma\rangle], \quad (5)$$

where $\varepsilon=\pm1$. For states of doublet spin multiplicity, the $\varepsilon=+1$ states are labeled e, and $\varepsilon=-1$ states, f.[25]

For a molecule in a $^2\Pi$ electronic state, in a Hund's case (a) basis, the spin–orbit term in the molecular Hamiltonian is diagonal, leading to a splitting between the $\Omega=1/2$ and 3/2 manifolds, whose magnitude is given by the spin–orbit constant, denoted $A_{\rm so}$.[22–24] Simultaneously, there exists a coupling between the $\Omega=1/2$ and 3/2 states due to the spin–rotation ($\mathbf{J}\cdot\mathbf{L}$) term which arises in the expansion of the $(\mathbf{J}-\mathbf{L}-\mathbf{S})^2/2\mu r^2$ term in Eq. (3).[22–24] For a molecule such as CH, where the rotational constant B is large with respect to $A_{\rm so}$, this mixing is significant. The true molecular wave functions in this intermediate case coupling are linear combinations of the case (a) wave functions

$$|JMF_i\varepsilon\rangle = \sum_{\Omega}\sum_{l=2}^{\infty}\left[\frac{(l-2)!}{(l+2)!}\right]^{1/2}P_l^2\sum_{M,m_L}C^{\Omega}_{JF_i\varepsilon}|JM\Omega\varepsilon\rangle. \quad (6)$$

The expansion coefficients $C^{\Omega}_{JF_i\varepsilon}$ are obtained by diagonalization of the molecular Hamiltonian.[22–24] Eigenfunctions of a given J and parity are conventionally labeled F_1, F_2 in order of increasing energy.[25] For the X state of CH, since the ratio of the spin–orbit constant $A_{\rm so}$ to the rotational constant B is less than 2, the $J=1/2$ levels, which can occur only with $\Omega=1/2$, are labeled F_2. Figure 1 illustrates the relative position and labeling of the rotational levels of the $X\,^2\Pi$ state of CH. The splitting between the e and f Λ doublet levels of each F_i level is too small to be shown in the figure. The N quantum number designates the sum of the rotational angular momentum and electronic orbital angular momentum. In Hund's case (b) $J=N\pm1/2$ for the F_1 and F_2 manifolds, respectively. Each rotational state of CH indexed by N comprises four separate states in two different spin–orbit manifolds indexed by F_i with one e and one f Λ-doublet level in each manifold.

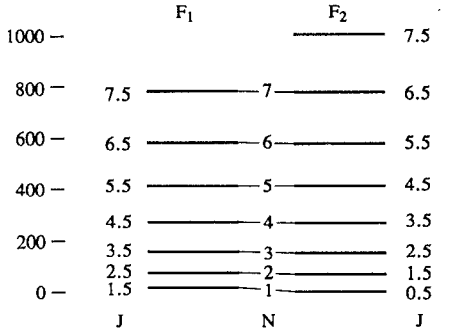

FIG. 1. Energy level diagram for the lowest rotational levels of CH ($X\,^2\Pi$) illustrating the assignment of the F_1 label and J and N quantum numbers. The spacing of the rotational levels is to scale, determined from the spectroscopic constants given in Ref. 40. The Λ doublet splitting, which is less than 1 cm^{-1}, is not indicated on the diagram.

In the case (b) limit, where $BJ\gg|A_{\rm so}|$, the expansion coefficients can be expressed as[26,27]

$$C^{\Omega}_{JF_i\varepsilon}=(-1)^{N-J+\Sigma}(JS\Omega-\Sigma\,|\,N\Lambda), \quad (7)$$

where $(\cdots|\cdots)$ is a Clebsch–Gordan coefficient[28] and $J=J\pm1/2$ for the F_2 and F_1 levels, respectively. In the high J limit,

This article is copyrighted as indicated in the article. Reuse of AIP content is subject to the terms at: http://scitation.aip.org/termsconditions. Downloaded to IP:

$$\lim_{J,N\gg 1} |C^{\Omega}_{JF_i\varepsilon}| = 2^{-1/2}, \tag{8}$$

so that the F_1 and F_2 wave functions will be an equal admixture of the case (a) $\Omega=1/2$ and $\Omega=3/2$ basis functions.

The approach of a spherical scattering partner will lift the twofold degeneracy of the Π electronic state of the diatomic, leading to electronic wave functions for the CH(X)+He system which are either symmetric (A') or antisymmetric (A'') with respect to reflection of the electronic spatial coordinates in the triatomic plane.[3,29,30] Two potential energy surfaces, $V_{A'}$ and $V_{A''}$, correspond to these two electronic states. These potential surfaces are functions of r, R, and θ.[3] It is most convenient to deal with the sum and difference of $V_{A'}$ and $V_{A''}$, which are expanded as[3]

$$\sum_{l=0}^{\infty} P_l(\cos\theta) V_{l0}(R,r) = (V_{A''}+V_{A'})/2, \tag{9}$$

and

$$\sum_{l=2}^{\infty} \left[\frac{(l-2)!}{(l+2)!}\right]^{1/2} P_l^2(\cos\theta) V_{l2}(R,r) = (V_{A''}-V_{A'})/2, \tag{10}$$

where $P_l(\cos\theta)$ and $P_l^2(\cos\theta)$ designate, respectively, regular and associated Legendre polynomials.

As anticipated above, to describe the collision one expands the wave function of the composite system consisting of the molecule and scattering partner in terms of products of molecular eigenfunctions and wave functions describing the relative orbital motion of the collision system.[2] This corresponds to the asymptotically correct description of the atom + diatom system. These product wave functions are chosen to be eigenfunctions of the total angular momentum J with spaced-fixed projection M,

$$|JF_iLJM\rangle = \sum_{M,m_L} (JMLm_L|JM)\,|JMF_i\varepsilon\rangle\,|Lm_L\rangle, \tag{11}$$

where L and m_L designate the orbital angular momentum of the collision pair and its spaced-fixed projection.

Transition probabilities and scattering amplitudes and cross sections can be evaluated by solution of the close coupled (CC) equations which arise when Eq. (11) is substituted into the Schrödinger equation.[2] To solve these equations one must first evaluate matrix elements of the interaction potential $V(r,R,\theta,\mathbf{q})$ in the intermediate coupling basis. For brevity we shall not reproduce these lengthy expressions here, but refer the interested reader to our earlier article.[16] Integral cross sections for transitions between individual $|JMF_i\varepsilon\rangle$ multiplet levels can be obtained in the usual manner from the asymptotic form of the solution to these CC equations.[2,16,31–33] Implicit in all earlier treatments is the assumption that the matrix elements of the terms $H_{so}(\mathbf{q};r)$ and $(\mathbf{J}-\mathbf{L}-\mathbf{S})^2/2\mu r^2$ in the molecular Hamiltonian [Eq. (3)] are *unchanged* from their values in the isolated diatomic. The possible implications of this assumption will be discussed in more detail below.

In the case (a) limit, in which Ω is a good quantum number, transitions between levels in the *same* spin–orbit manifold ($\Omega'=\Omega$) will be coupled only by the $V_{l0}(R,r)$ terms in the expansion of the potential [Eq. (9)], while transitions between levels in *different* spin–orbit manifolds ($\Omega'\neq\Omega$) will be coupled only by the $V_{l2}(R,r)$ terms in the expansion of the potential [Eq. (10)]. In other words, inelastic transitions within a given spin–orbit manifold will be sensitive to the *average* of the $V_{A'}$ and $V_{A''}$ potential energy surfaces, while inelastic transitions from one spin–orbit manifold to the other will be sensitive to the *difference* between the $V_{A'}$ and $V_{A''}$ potentials.

In the intermediate coupling and case (b) limits, the mixing of the case (a) basis states [Eq. (4)] implies that transitions between any pair of $|JMF_i\varepsilon\rangle$ multiplet levels will be coupled by *both* the $V_{l2}(R,r)$ terms and $V_{l0}(R,r)$ terms in the expansion of the potential. These terms will add constructively or destructively, depending on the initial and final multiplet labels.[16] The magnitude of the resulting cross sections will be sensitive to this quantum interference, so that the simple case (a) propensity rules[2] will no longer be valid. As we have shown,[16,34] depending on the sign of the difference between $V_{A'}$ and $V_{A''}$ one can in some cases predict a propensity for selective populations of final states which are either *symmetric* (A'; F_1e or F_2f) or *antisymmetric* (A''; F_1f or F_2e) with respect to reflection of the spatial part of the electronic wave function in the plane of rotation of the CH molecule.

In most of the calculations to be discussed here, the CH molecule is treated as a rigid rotor, and the interaction potential is not averaged over the vibrational motion of the CH molecule. Unless otherwise mentioned, the variable r which appears in Eqs. (9) and (10) is held equal to the equilibrium internuclear distance of the isolated CH molecule, as calculated with the *ab initio* potential, namely, $r=2.1108$ bohr. This value differs insubstantially from the experimental equilibrium value of 2.1163 bohr.[35]

III. DETERMINATION OF CROSS SECTIONS

The *ab initio* potential energy surfaces described in Paper I were used in the present scattering calculations. These surfaces involved multiparameter fits made to about 200 calculated points. The "standard" potential energy surface in Paper I will be designated as TZP. Unless otherwise indicated, this is the surface used in the scattering calculations and is the only one used in Sec. IV. Three other surfaces are also developed in Paper I. They are designated as QZP, QZPDC, and PWII and differ from the standard surface in the size of atomic orbital basis set, in the selection procedure in the configuration interaction, and in the flexibility of the functional form used to represent of the calculated points as a continuous surface. These three alternative surfaces will be used in selected scattering calculations discussed in Sec. V.

The scattering calculations were carried out using the HIBRIDON package of Alexander and co-workers.[36] Calculations were performed using the exact coupled channel (CC) formulation without any dynamical approximations, at total energies chosen on two different grids. The denser

This article is copyrighted as indicated in the article. Reuse of AIP content is subject to the terms at: http://scitation.aip.org/termsconditions. Downloaded to IP: 141.209.100.60 On: Mon, 22 Dec 2014 16:43:09

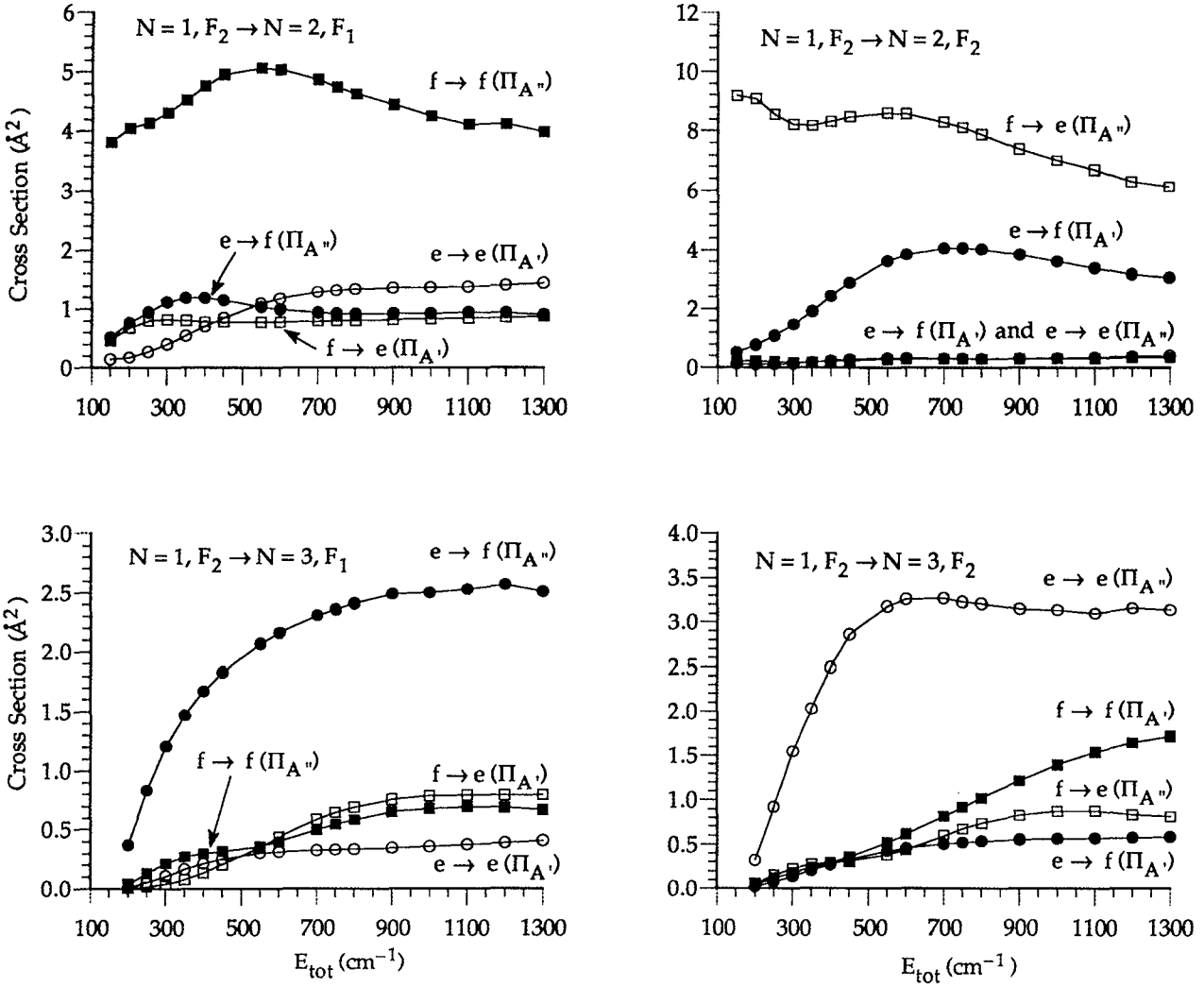

FIG. 2. Integral cross sections out of the $N=1$, F_2e and $f\Lambda$ doublet levels ($J=1/2$, e/f) into (upper left panel) the $N=2$, $F_1\Lambda$ doublet ($J=3/2$); (upper right panel) the $N=2$, $F_2\Lambda$ doublet ($J=5/2$); (lower left panel) the $N=3$, $F_1\Lambda$ doublet ($J=5/2$); (lower right panel) the $N=2$, $F_2\Lambda$ doublet ($J=7/2$).

grid has energies of 200–800 cm^{-1} in increments of 50 cm^{-1}, and 900–1400 cm^{-1} in increments of 100 cm^{-1}. The sparser grid has energies of 175, 280, 437, 612, 700, 875, 1225, and 1400 cm^{-1}, corresponding to 0.5, 0.8, 1.25, 1.75, 2.0, 2.5, 3.5, and 4.0 kcal/mol, a selection particularly appropriate for comparison to experiment. While more compact and therefore less computationally demanding, the use of the sparser grid does lead to slight artificial undulations in the spline interpolation of a few of the resulting cross sections as a function of energy. The integration parameters, the number of partial waves included, and the maximum rotational level included in the channel basis were all adjusted to ensure convergence of the calculated inelastic integral cross sections to within a few percent.

IV. INTEGRAL CROSS SECTIONS

Integral cross sections for transitions out of the $N=1$ F_1e and f levels ($J=1/2$ $\varepsilon=\pm1$) into all four levels with $N=2$ and 3 are shown as a function of the energy in Fig. 2. The cross sections all are smooth functions of the energy, with no evidence of resonance structures or oscillations. The curves all rise smoothly from threshold to a plateau at high energy. The values of the cross sections at $E=1000$ cm^{-1} are identical to those given in Table II of Ref. 16.

The variation of the magnitudes of the scattering cross sections with the initial and final Λ-doublet level is of considerable interest. In the case (a) limit, for a given initial J and Ω and a given final J' and Ω', the cross section for the $\varepsilon\rightarrow\varepsilon'$ transition will be identical to that for the $-\varepsilon\rightarrow-\varepsilon'$ transition. As discussed above, the case (a) propensity rules no longer apply in intermediate or case (b) coupling. It is clear from Fig. 2 that, at least for transitions with $\Delta N=1$ and 2, one of the four cross sections is dominant. To gain more insight, we have also computed *fine-structure propensities*, defined by Liu and Macdonald[18,19] as

$$P_{fs}(NF\varepsilon;N'F'E)=\sum_{\varepsilon'}\sigma(N'F'\varepsilon'\rightarrow NF\varepsilon;E)$$

This article is copyrighted as indicated in the article. Reuse of AIP content is subject to the terms at: http://scitation.aip.org/termsconditions. Downloaded to IP: 141.209.100.60 On: Mon, 22 Dec 2014 16:43:09

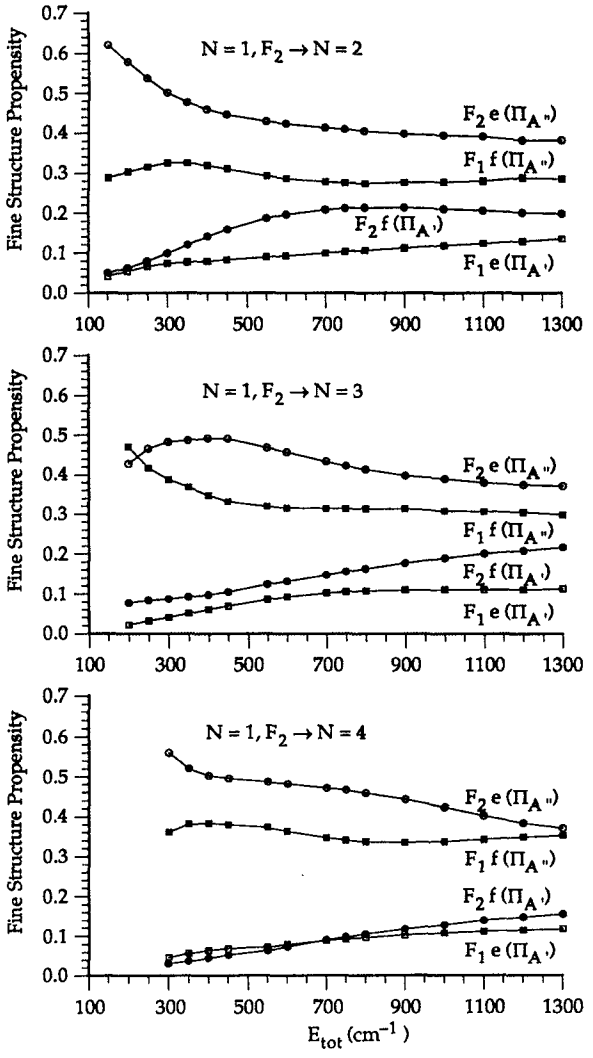

FIG. 3. Fine structure propensities [defined in Eq. (12)] for transitions out of $N=1$, $F_2(J=1/2, F_2)$ into the $N=2$, $N=4$, and $N=5$ levels.

$$\times\left[\sum_{F,\varepsilon,\varepsilon'}\sigma(N'F'\varepsilon'\rightarrow NF\varepsilon;E)\right]^{-1}. \tag{12}$$

Here E denotes the *total* energy. Fine-structure propensities are plotted in Fig. 3, for transitions out of the $N=1$, F_2 level (Fig. 1) into the $N=2$, 3, and 4 levels. We see here, in full agreement with the experimental findings of Macdonald and Liu,[18,19] that transitions are preferred into final states in which the electronic wave function is *antisymmetric* with respect to reflection in the plane of rotation of the molecule.

In previous work[16] we demonstrated that for collisions between a noble gas atom and a molecule in a Π electronic state arising from a π^1 orbital occupancy, as is the case for CH($X\,^2\Pi$), *upward* transitions ($J_{\text{final}}>J_{\text{initial}}$) into final states of A'' reflection symmetry—F_1f and F_2e—should be prefered over transitions into final states of A' reflection symmetry. This was a consequence of a more repulsive interaction between the incoming noble gas atom and the lone π orbital when that orbital lies in the triatomic plane. Although our earlier analysis focused on the relative size of the cross sections for transitions into the four possible multiplet levels for a given final value of J, we see in Figs. 2 and 3 that the same conclusions apply to the four cross sections for a given final value of N.

TABLE I. Relative populations of rotational levels in the incident CH beam in the experiments of Macdonald and Liu (Refs. 18 and 19). The upper and lower entries, for each N, correspond, respectively, to the e and f levels.

N	F_1	F_2
1	0.166 31	0.784 73
	0.166 31	0.784 73
2	0.010 83	0.014 97
	0.012 23	0.012 63
3	0.002 63	0.002 63
	0.001 83	0.002 24
4	0.000 72	0.000 64
	0.000 54	0.000 82
5	0.000 34	0.000 18
	0.000 21	0.000 30
6	0.000 13	0.000 10
	0.000 08	0.000 17
7	0.000 09	0.000 04
	0.000 04[a]	0.000 09[a]
8	0.000 06	0.000 03
	0.000 03	0.000 05
9	0.000 18	0.000 03
	0.000 03	0.000 15
10	0.000 24	0.000 02
	0.000 03	0.000 15

[a]Because of spectral overlap, the populations in the $N=7f$ labeled levels could not be determined experimentally. The tabulated values represent a linear interpolation from the corresponding f labeled levels for $N=6$ and $N=8$.

V. COMPARISON WITH EXPERIMENT

The experiments of Macdonald and Liu[18,19] measured transitions into all four states associated with $N=3$–7 over collision energies ranging from roughly 150 to 1400 cm^{-1}. A direct comparison between calculated quantities and those measured experimentally involves three additional transformations of the calculated data.

First, the computed cross sections into any given final state must be averaged over the distribution of initial states present in the incident CH beam. The resulting effective cross sections, which are the quantities measured experimentally, can be written as

$$\sigma(NF\varepsilon;E_t)=\sum_{N',F_i',\varepsilon'}P(N'F_i'\varepsilon')\times\sigma(N'F_i'\varepsilon'\rightarrow NF\varepsilon;E_t+e_{N'F_i'\varepsilon'})\times\left[\sum_{N',F_i',\varepsilon'}P(N'F_i'\varepsilon')\right]^{-1}, \tag{13}$$

where $P(N'F_i'\varepsilon')$ designates the relative population of state $N'F_i'\varepsilon'$ in the incident beam and E_t and $e_{N'F_i'\varepsilon'}$ denote, respectively, the initial translational energy and the

This article is copyrighted as indicated in the article. Reuse of AIP content is subject to the terms at: http://scitation.aip.org/termsconditions. Downloaded to IP: 141.209.100.60 On: Mon, 22 Dec 2014 16:43:09

internal energy of state $N'F_i'\varepsilon'$. The relative populations in the beam are given in Table I. As can be seen, ~78% of the beam is in the $J=0.5$, F_2 Λ doublet, with an additional ~17% in the $J=1.5$, F_1 Λ-doublet—thus a total of ~95% in the $N=1$ levels. From Eq. (13), for a given translational energy, the effective cross sections represent a sum over many different total energies. The required values were obtained by spline interpolation of the calculated integral cross sections, determined on the grid of energies mentioned above.

Second, in the experiments of Macdonald and Liu the collision energy is selected by varying the crossing angle of two supersonic molecular beams each of which has a finite beam divergence and velocity distribution. Consequently, the experimental cross section at each nominal collision energy represents, in reality, a complicated average over a distribution of translational energies. The experimentally determined[37] velocity distributions have a full width at half maximum ranging from about 10% of the nominal value at high velocity up to 20% at low velocity. Tests performed by velocity averaging the theoretical cross sections of Eq. (13) over a Gaussian distribution with these widths indicated that such averaging has a negligible effect on the final cross sections, except very close to threshold, and, further, would not affect any of the conclusions presented below. Consequently, for convenience, this additional velocity averaging was not carried out systematically.

Third, the experimental values are obtained only as *relative* values. Therefore, the experimental cross sections were multiplied by a single constant scale factor K. Although the size of the measured cross sections vary by about one and a half orders of magnitude, the experimental error in each measurement is thought[37] to be an approximately constant relative error. On this basis, the scale factor was chosen to minimize the *relative* error between experiment and theory, namely,

$$\Delta=\sum\left[1-\sigma(NF\varepsilon;E_t)/\{K\sigma^{\exp}(NF\varepsilon;E_t)\}\right]^2, \qquad (14)$$

where the sum runs over all the experimental data points. Obviously, this type of comparison can emphasize deviations between theory and experiment for cross sections which are quite small on an absolute scale while deemphasizing differences between the larger cross sections.

The theoretically determined $\sigma(NF\varepsilon;E_t)$ cross sections and the scaled experimental values are compared, as a function of collision energy, in Figs. 4–6. In Fig. 4, the cross section for the one multiplet level for each N which was experimentally determined over the largest energy range is displayed for all available values of N. The lowest energetic threshold of any component of a given N is indicated at the base of the figure. Figure 5 is a similar plot where all four components of each N have been summed. The energy range for the experimental results in Fig. 5 is reduced from that of Fig. 4 because cross sections for transitions into all multiplet levels for each N were not measured over comparable ranges. In Fig. 6 we plot the ratios of various multiplet resolved cross sections into $N'=3$, 4, 5, 6, and 7 as a function of energy. For each N there exist

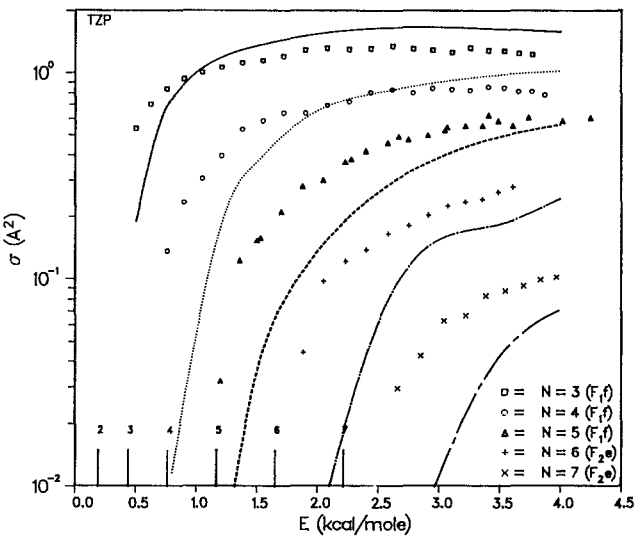

FIG. 4. Comparison of normalized experimental (symbols) and appropriately averaged calculated (solid curves) cross sections for transitions into individual rotational levels of CH, summed over all four multiplet levels for a given N, as a function of relative translational energy. The theoretical state-to-state cross sections were averaged over the experimental distribution of initial rotational state [see Eq. (13) and Table I]. The experimental cross sections were normalized by multiplication by a single constant factor, as defined in Eq. (14). For each N, the threshold for the lowest multiplet level is indicated by the vertical bars.

three independent ratios which are displayed as separate panels in the figure. Within each panel, the arrow indicates the energetic threshold. The panel marked F_1e/F_2f is the ratio of the two cross sections into final states of A' reflection symmetry. The panel marked F_2e/F_1f is the ratio of

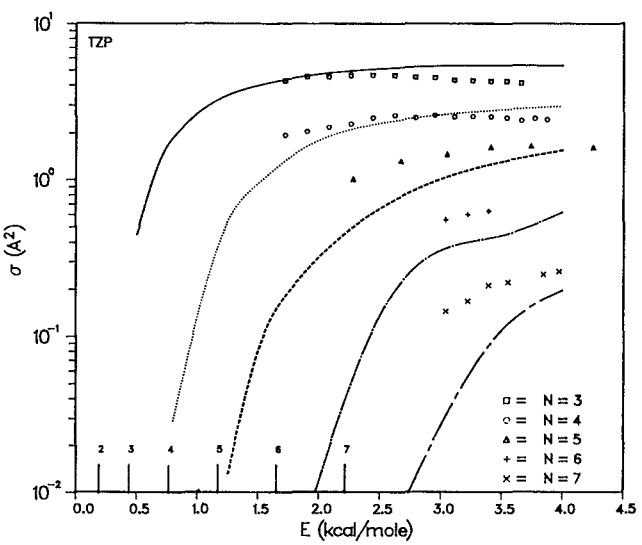

FIG. 5. Comparison of normalized experimental (symbols) and appropriately averaged calculated (solid curves) cross sections for transitions into selected individual multiplet components of each rotational state of CH, as a function of relative translational energy. The theoretical state-to-state cross sections were averaged over the experimental distribution of initial rotational states [see Eq. (13) and Table I]. The experimental cross sections were normalized by multiplication by a single constant factor, as defined in Eq. (14). The thresholds for all the multiplet levels considered are indicated by the vertical bars.

This article is copyrighted as indicated in the article. Reuse of AIP content is subject to the terms at: http://scitation.aip.org/termsconditions. Downloaded to IP: 141.209.100.60 On: Mon, 22 Dec 2014 16:43:09

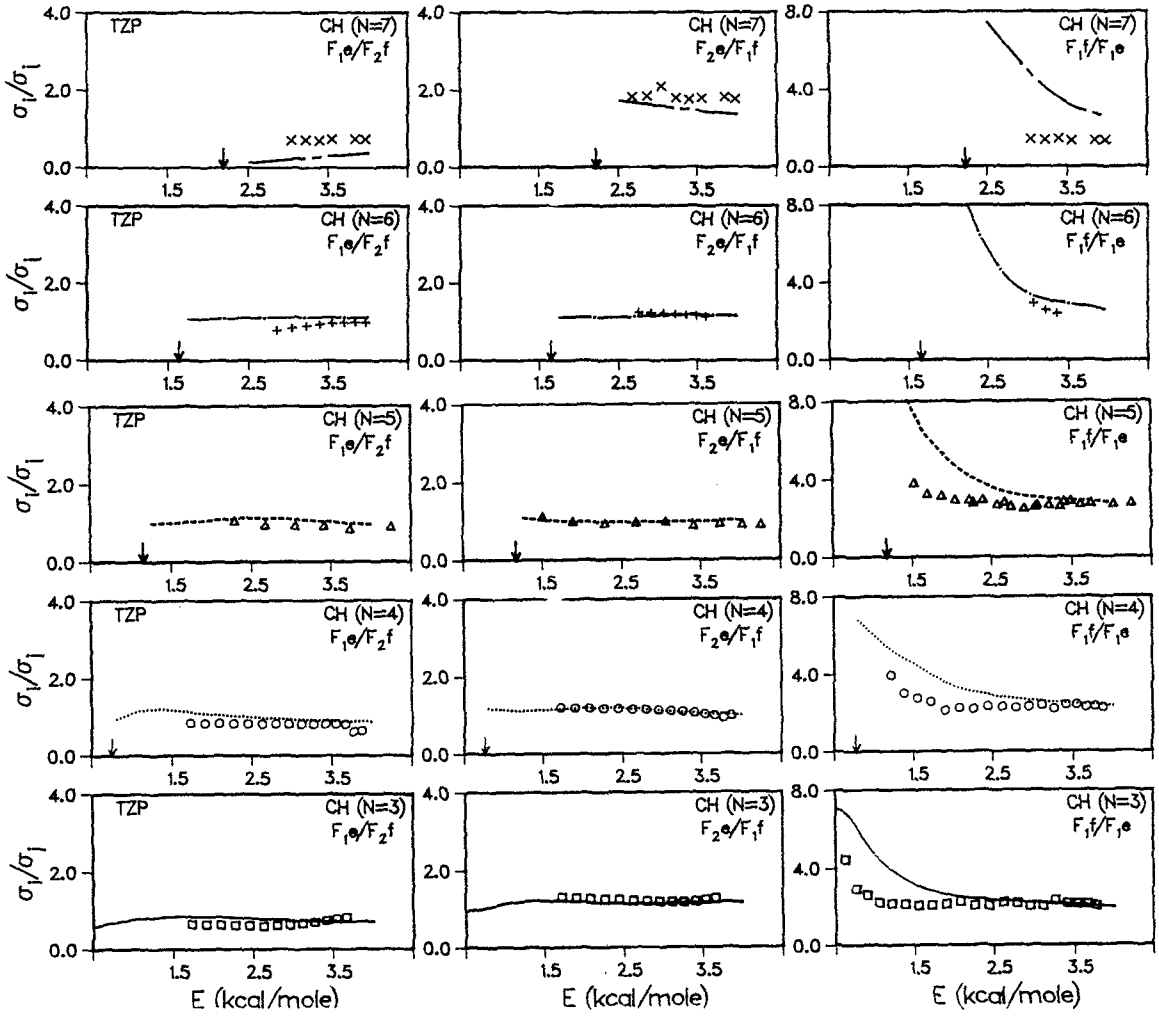

FIG. 6. Comparison of experimental (symbols) and appropriately averaged calculated (solid curves) ratios of cross sections for transitions into the labeled multiplet components of each rotational state of CH, as a function of relative translational energy.

the cross sections into states of A'' symmetry. The final panel, marked F_1f/F_1e, is the ratio of cross sections for transitions into one A'' and one A' level. Figures 4–6 represent a complete comparison between theory and experiment; no experimental data point has been omitted.

Overall, the agreement between calculated and experimental values is good. In particular, the third panel for each N in Fig. 6 reaffirms the propensity (and for higher values of N than contained in Fig. 3) for transitions into final states of A'' reflection symmetry and displays the experimental confirmation of this propensity. However, there are significant and systematic qualitative differences between theory and experiment. In both Figs. 4 and 5, the calculated cross sections show a dynamic threshold at the limit of experimental detectability that is increasingly higher than the energetic threshold as N increases. In contrast, the experimental values go directly to the energetic threshold and, in some cases, a lower threshold due to the velocity spread in the incident beams. As mentioned above, the discrepancy is not significantly reduced by averaging of the theoretical results over a Gaussian velocity distribution chosen to simulate the experimental velocity spread.

The experimental results in Figs. 4 and 5 also show a perceptible peaking of the cross section for the lower values of N within the observable energy range. This peaking is much less pronounced or entirely absent in the theoretical results.

In sum, then, the theoretical cross sections rise more slowly and over a broader energy range to peak at about the correct relative size but at a higher value of the energy than observed experimentally. Figure 6 indicates that theory does correctly preserve the nearly energy independent ratio between the cross sections into either the two A' or the two A'' multiplet levels for a given N. However, near threshold the theoretical calculations predict a much stronger propensity for transitions into the A'' levels than found experimentally. The cross sections displayed in the comparison in Fig. 4 all refer to transitions into levels of A'' symmetry. The results of Figs. 4 and 6 taken together indicate that a plot similar to Fig. 4 but for transitions into levels of A' symmetry would show even larger deviations from experiment near threshold.

In order to put the significance of these disagreements in better perspective, it is worthwhile to consider the mag-

This article is copyrighted as indicated in the article. Reuse of AIP content is subject to the terms at: http://scitation.aip.org/termsconditions. Downloaded to IP: 141.209.100.66 On: Mon, 22 Dec 2014 16:45:09

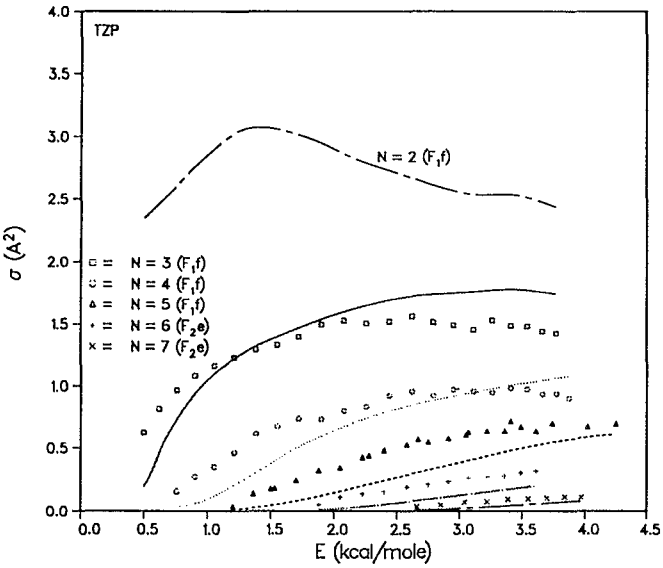

FIG. 7. Indentical to Fig. 5 but plotted on a linear scale and including the appropriately averaged calculated cross section for transition into the $N=2$, F_1, e level of CH, as a function of relative translational energy.

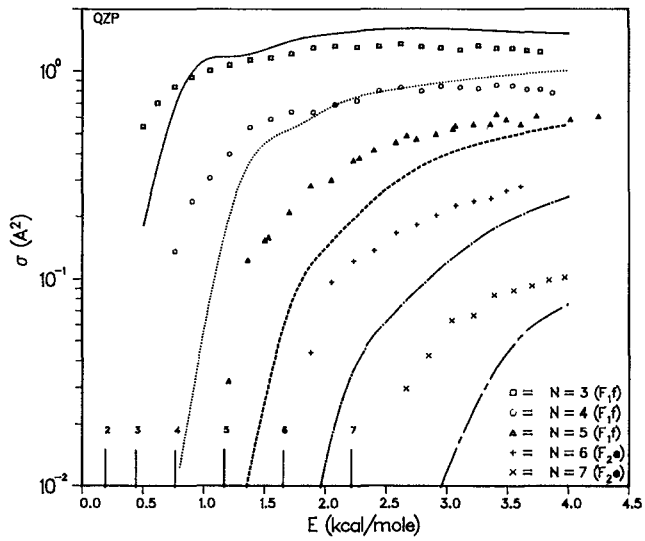

FIG. 8. As in Fig. 5 but for calculations on the QZP surfaces.

nitude of the differences compared to the effective cross sections into levels with $N=2$, which dominate the total inelastic cross sections. Unfortunately, cross sections for transitions into $N=2$ could not be determined experimentally, because of the significant population of these levels in the initial beam. Figure 7 displays cross sections averaged over initial states identical to Fig. 5, but with the addition of the calculated cross sections into the $N=2$, F_1f level. This figure is also plotted on an absolute scale and, for this one figure alone, the scale factor for normalizing the experiment was determined by minimizing the *absolute* error. In this form, the theoretical discrepancies with experiment appear to be at most on the order of 5% of the total inelastic cross sections. Certainly, when represented in this manner, the overall comparison between experiment and theory is good. Notwithstanding, in the remainder of this paper we shall focus on the possible origins of the small but systematic errors revealed in the comparisons between theory and experiments on a relative scale embodied in Figs. 4–6.

VI. SENSITIVITY TO APPROXIMATIONS IN THE CALCULATION

In order to determine if approximations in the *ab initio* calculation of the potential energy surfaces or dynamical approximations in the scattering calculations were the source of the disagreement with experiment, a series of diagnostic calculations were performed.

We considered first systematic errors in the potential energy surfaces. As described in detail in Paper I, the approximations in determining the surface come in one of three forms: too simple a basis set, too limited a configuration interaction, and too simple a functional form used in constructing a global representation of the discrete set of *ab initio* points. Compared to the "standard" TZP surfaces used in the preceding section, the QZP surfaces are built on a more complete atomic orbital basis, and the QZPDC surfaces include, in addition, a more extended configuration interaction treatment of dynamic correlation. By contrast, the PWII surfaces are built on the identical points used in constructing the TZP surfaces, but involve a considerably simplified fitting function. In addition, the PWII surfaces eliminate entirely the small van der Waals features of the TZP surfaces, features that are probably only qualitatively described in the TZP, QZP, and QZPDC surfaces (for reasons discussed in Paper I). Repeating the calculations in the preceding section with each of these alternative surfaces (PWII, QZP, and QZPDC) should expose those features of the calculated cross sections which are most sensitive to the approximations in the potential energy surfaces.

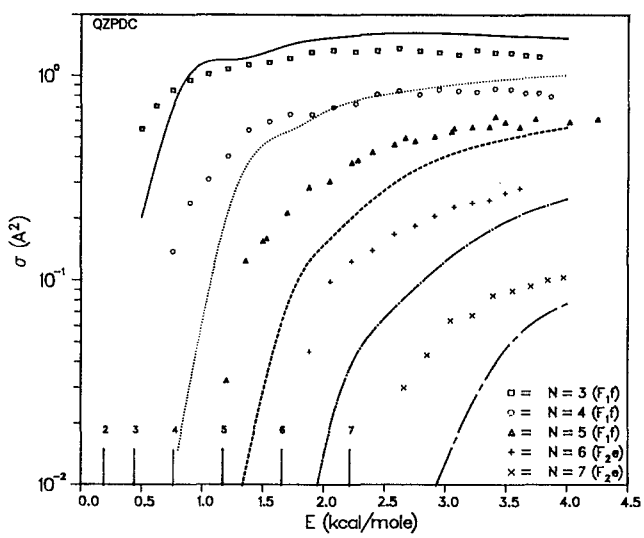

FIG. 9. As in Fig. 5 but for calculations on the QZPDC surfaces.

This article is copyrighted as indicated in the article. Reuse of AIP content is subject to the terms at: http://scitation.aip.org/termsconditions. Downloaded to IP: 141.209.100.60 On: Mon, 22 Dec 2014 16:43:09

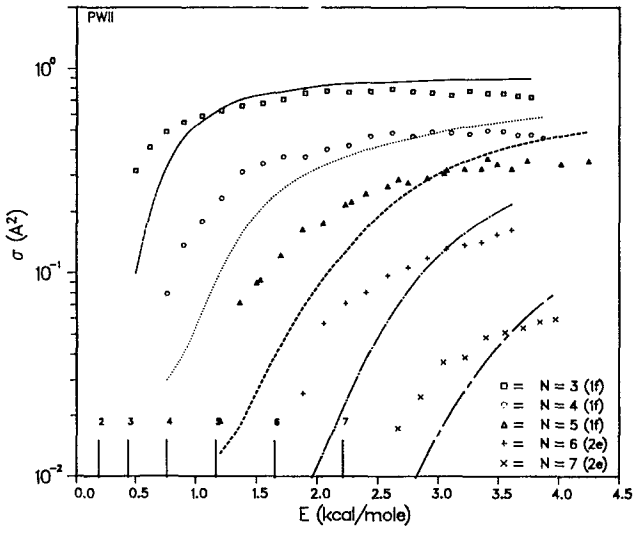

FIG. 10. As in Fig. 5 but for calculations on the PWII surfaces.

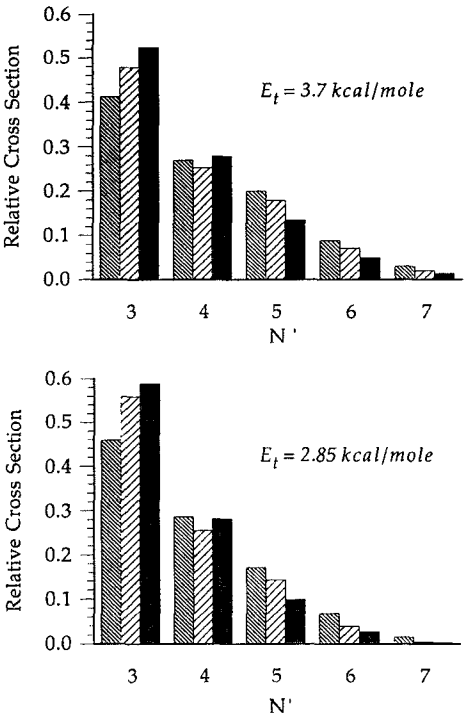

FIG. 11. Comparison of *relative* cross sections normalized to a unit sum for selected transitions into the $N=3$, 4, 5 F_1f and $N=6$, 7 F_2e levels for initial translational energies of 1000 and 1300 cm^{-1}. The left histogram represents the experimental results while the middle and right histograms represent the theoretical results from, respectively, the TZP surfaces (used in Figs. 4–6) and the PWII surface (used in Fig. 10).

Qualitatively, the cross sections calculated on each of these three alternative surfaces are quite similar to one another and to the results on the standard surfaces. This is illustrated by Figs. 8–10 which replicate Fig. 4 for the QZP, QZPDC, and PWII surfaces, respectively. While there are some differences between Figs. 4 and 8–10, all show similar threshold behavior and the absence of peaking in the cross sections over the range of collision energies sampled in the experiments. From one point of view, these results are quite gratifying. The differences between the TZP, QZP, QZPDC surfaces are at most small fractions of a kcal/mol (see Paper I) over the range of energies (up to 4 kcal/mol) sampled in the experiment. If higher accuracies than this were required, it would indeed make it especially difficult to calculated accurate potential energy surfaces for hydride–noble gas systems.

The agreement between the cross sections shown in Fig. 4 and the PWII values in Fig. 10 is also satisfying, at least qualitatively. As discussed in Paper I, the PWII surfaces have only 11 adustable parameters, almost *one order of magnitude* fewer than the number used to fit the other surfaces. The PWII surfaces retain correct shapes and are based on a physically intuitive, rather than mathematically complete, form. The rms error between this function and the calculated points is about an order of magnitude *higher* than in the case of the TZP, QZP, and QZPDC surfaces and the small van der Waals features seen in these other surfaces are completely absent. Notwithstanding, the cross sections displayed in Fig. 10, in comparison to those in Fig. 4, indicate that the *relative* degree of agreement with experiment is not significantly altered while the overall magnitude of the calculated cross sections is significantly reduced, by a factor of 2. In Fig. 11, the *relative* cross sections, normalized to a unit sum, for scattering into the $N=3$, 4, 5 F_1f and $N=6$, 7 F_2e levels is displayed for the calculations with the TZP and PWII surfaces and the corresponding experimental results at relative translational energies of 2.85 and 3.7 kcal/mol (1000 and 1300 cm^{-1}). The similarity between the two different calculations is clearly evident. The results in Fig. 11 are plotted on a linear scale and again emphasize that, overall, the *relative* dependence of the cross sections on final state is being correctly predicted by the calculations on the PWII potential surfaces. However, if the experimental results were available on an absolute basis, the PWII would be clearly deficient.

Since the van der Waals features are present on the TZP, QZP, and QZPDC surfaces but are absent on the PWII surfaces, it can be argued that these features have no qualitative effect on the agreement between theory and experiment. However, the first three sets of surfaces *underestimate* the van der Waals feature (see Paper I). To gauge the importance of deeper van der Waals wells, a highly approximate IOS/JWKB inelastic scattering calculation[38] was performed on an adjustable model of the *average* potential energy surface. The use of the average potential approximates the reactants as closed shell species. The IOS approximation works less well for hydrides, such as CH, because their rotational periods are fast. Nonetheless, the dynamical effects of an extensive array of van der Waals features can be quickly assessed. These calculations indicate that van der Waals features noticeably increase inelastic scattering over a range of collision energies approximately three times the van der Waals well depth. Since the van der Waals features on the TZP average potential varies with angle from 0.015 to 0.045 kcal/mol, the model calcu-

This article is copyrighted as indicated in the article. Reuse of AIP content is subject to the terms at: http://scitation.aip.org/termsconditions. Downloaded to IP: 141.209.100.60 On: Mon, 22 Dec 2014 16:43:09

lations conclude that even doubling the size of the well would produce no noticeable increase in the cross section 0.1 to 0.3 kcal/mol beyond the energetic threshold. Such improvement would not be visible in Fig. 4 for the higher rotational states. Thus these highly approximate calculations indicate the van der Waals features do not qualitatively influence agreement between theory and experiment.

Since the consequences of variations in the potential energy surfaces suggest no explanation for the observed discrepancies between theory and experiment, we were led to speculate on the effects of approximations in the scattering calculations. As discussed in Sec. II, these are of two forms: (1) the rigid-rotor approximation and (2) the assumption, mentioned earlier, that the matrix elements of the non-Born–Oppenheimer terms $(\mathbf{J}-\mathbf{L}-\mathbf{S})^2/2\mu r^2$ and $H_{so}(\mathbf{q};r)$ in the molecular Hamiltonian are *unchanged* from their values in the isolated diatomic. In other words, the perturbation of the electronic wave function of the CH molecule which accompanies the approach of the helium atom is assumed to affect insignificantly both the spacing of the $^2\Pi$ multiplet levels and the degree of mixing of the case (a) functions which compose the CH wave functions [Eq. (6)] which enter into the expansion of the scattering wave function [Eq. (11)].

We examine first the rigid-rotor approximation, within which the CH bond distance in Eqs. (9) and (10) is held equal to the equilibrium internuclear separation of the isolated CH molecule. Since the range of energies sampled experimentally is too low to allow vibrational excitation, the expectation would be that this approximation should be reasonably accurate. Nonetheless, we have carried out two variations in order to examine the effects of the vibrational motion of the CH molecule on the calculated *rotationally inelastic* cross sections. First, we fixed r at the outer turning point of the $v=0$ vibrational level of CH rather than at its equilibrium distance (2.347 bohr as compared to 2.111 bohr). Second, rather than keeping r fixed at a constant value, we varied it at each CH–He distance R to be equal to the equilibrium internuclear distance at that particular R (averaged over CHHe angle). This is the vibrationally adiabatic potential energy surfaces labeled TZPA in Paper I. These limiting surfaces simulate the average coupling between the vibrational motion and rotational inelasticity while the outer turning point approximation models the extremum of the vibrational modulation of the collision frame dynamics. The results of either of these two variations are very similar to each other and to the results for the standard calculations. Because of the similarity no results are plotted. Neither approximation improved agreement with experiment significantly, indicating that the neglect of the vibrational motion of the CH molecule is not a likely origin of the disagreement, seen in Figs. 4 and 5, between the theoretical predictions and experimental measurements of the energy dependence of the inelastic cross sections.

We now consider a possible breakdown in the approximation that the matrix elements of the non-Born–Oppenheimer operators in the molecular Hamiltonian are unaffected by the approach of the He atom. Since the $V_{A'}$ and $V_{A''}$ potentials discussed in Sec. II differ so greatly in their rotational anisotropy and since the degree of mixing between the case (a) wave functions in a $^2\Pi$ molecule is strongly dependent on the spin–orbit spacing in the diatomic,[24] one might imagine that a geometry-dependent change in the spin–orbit constant could expose the scattering flux to the more anisotropic difference potential and thus result in cross sections with higher levels of rotational scattering at lower collisional energies. This could result in improved agreement between theory and experiment. One might further expect that for any changes in the constants to significantly affect the dynamics, they must occur at geometries where the changes in the values are comparable to the difference potential. At close-in geometries, where the A' and A'' surfaces are considerably different from one another, even *relatively* large changes in the small constants would be expected to have marginal dynamical effects.

Unfortunately, little is known quantitatively about the scale of the geometry dependence of the matrix elements of either the spin–orbit operator or the various other terms which result from the expansion of $(\mathbf{J}-\mathbf{L}-\mathbf{S})^2$. One relevant piece of information comes from spectroscopic experiments on Ar–OH complexes, where Lester and coworkers[39] have shown that the spin–orbit constant in the complex varies by as much as 10% from the value in free OH. The van der Waals regions of the CH+He surfaces show considerable difference between the A' and A'' in a qualitative sense (much more so than in Ar–OH[10,11]). Nonetheless, the van der Waals region is so shallow that the absolute size of the difference potential is still quite small (on the order of 10 cm^{-1}). Thus relative changes in the spin–orbit constant comparable to those found in Ar–OH could perhaps have an effect.

The changes in the calculated cross sections due to a possible variation in the spin–orbit constant were examined using the following model: The spin–orbit constant A_{so}, which determines the splitting between the definite Ω case (a) levels,[24] was allowed to vary as a function of the interparticle distance R by replacing $H_{so}(\mathbf{q};r)$ in Eq. (3) by

$$H_{so}(\mathbf{q};r,R,\theta)=A_{so}(R=\infty)[1\pm 22.5\exp(-R)]\Lambda\cdot\Sigma, \tag{15}$$

where $A_{so}(R=\infty)\ \Lambda\cdot\Sigma$ is the spin–orbit operator in the isolated CH molecule.[22–24] The exponential term causes a progressive increase (or decrease) of the spin–orbit constant which rises from $\pm 2\%$ at $R=7$ bohr to $\pm 25\%$ at $R=4.5$ bohr. The latter value corresponds closely to the innermost classical turning point of the CH–He motion. No attempt was made to model a variation in the dependence of the spin–orbit constant on the CHHe angle. Since there is no angular dependence, the spin–orbit Hamiltonian is still diagonal in J, with matrix elements in the definite-parity Hund's case (a) basis [Eq. (5)] of

$$\begin{aligned}&\langle J'M'\Omega'\varepsilon'|H_{so}(\mathbf{q};r,R,\theta)|JM\Omega\varepsilon\rangle\\&\quad=\delta_{JJ'}\delta_{MM'}\delta_{\Omega\Omega'}\delta_{\varepsilon\varepsilon'}(1-\Omega)A_{so}(R),\end{aligned} \tag{16}$$

where

This article is copyrighted as indicated in the article. Reuse of AIP content is subject to the terms at: http://scitation.aip.org/termsconditions. Downloaded to IP:

$$A_{so}(R)=A_{so}(R=\infty)[1\pm 22.5\exp(-R)]. \quad (17)$$

Calculations with this R-dependent spin–orbit Hamiltonian, with both the + and − signs in Eq. (17), were carried out at total energies of 400 and 1000 cm^{-1}. The changes in the inelastic cross sections out of the $N=1$, F_2 levels ($J=1/2$, F_2) were everywhere less than 1%. One possible explanation of the observed insensitivity to variations in A_{so} is that since the rotational constant of CH is so large compared to the spin–orbit splitting, the molecule is virtually in the pure case (b) limit. Thus small changes in the spin–orbit coupling constant will have little effect on the case (a) mixing coefficients in Eq. (6). Consequently, the dependence of the calculated cross sections on the multiplet labels of the initial and final states (which, as we have seen, are sensitive to quantum interference induced by this mixing) will be little affected by small changes in A_{so}.

These results, taken with the results from the models of vibrational effects, strongly suggest that the disagreement with experiment does not have an obvious source in a small defect in the close-coupled dynamical approximations. However, it still might be that the rotationally inelastic cross sections could be sensitive to either the dependence of the matrix elements of the spin–orbit operator on the CH–He *angle*, or to the dependence on geometry of the other terms in the expansion of $(\mathbf{J}-\mathbf{L}-\mathbf{S})^2$. In principle, by adapting existing formalism for the treatment of the spectroscopy of $^2\Pi$ states of triatomic molecules,[40] the effect on the calculated cross sections of the variation of these small non-Born–Oppenheimer terms could be determined exactly. This would require, however, the prior determination of the geometry dependence of the matrix elements of terms such as $\mathbf{L}\cdot\mathbf{S}$, $\mathbf{L}^2$, $\mathbf{J}\cdot\mathbf{L}$, evaluated for the complete electronic wave functions of the CH–He system. This would, however, render the *ab initio* task more difficult.

VII. SUMMARY AND CONCLUSIONS

We have reported a series of full close-coupling calculations of integral cross sections for transitions between fine structure states of CH($X\,^2\Pi$) induced by collisions with He. These calculations were based on extensive prior *ab initio* investigations of the two CH($X\,^2\Pi$)+He potential energy surfaces (reported in the preceeding paper). The calculated cross sections from the $N=1\rightarrow N=2$, 3 levels confirmed a previous prediction of a propensity for preferential population of final state levels in which the electronic wave function of the CH molecule is *antisymmetric* with respect to reflection in the plane of rotation of the molecule.

Comparison between the energy-dependent cross sections determined in earlier experiments of Macdonald and Liu and appropriate averages of the calculated cross sections revealed generally good overall agreement. At all energies the discrepancies were everywhere less than 10% of the total inelastic cross sections. Nevertheless, the calculated cross sections tended to *underestimate* the degree of rotational inelasticity at low energy and *overestimate* it at higher energies. These differences persisted even after extensive investigation of the probable effect of correcting the remaining approximations in the theoretical treatment of the collision dynamics.

A cruder fit to the *ab initio* points was also tried, which completely ignores the van der Waals well region of the potential but is based on a very simple pairwise additive potential that correctly preserves the shape of the surfaces. The corresponding cross sections displayed a similar energy dependence to those calculated with the original fit, but with overall magnitudes which were a factor of 2 smaller. Nevertheless, because absolute values of the inelastic cross sections were not determined experimentally, both sets of theoretical cross sections yielded an equally satisfactory fit to experiment.

From a theoretical point of view, this series of calculations suggests that the resolution of the current discrepancy with experiment may require a more precise investigation of how the approach of the collision partner affects the electronic matrix elements of the non-Born–Oppenheimer terms in the molecular Hamiltonian. A second, but less likely, explanation is that more accurate and pronounced van der Waals wells may improve the agreement. (Approximate inelastic scattering calculations suggest any realistic van der Waals well is too small to have a qualitative effect.)

Finally, the availability from experiment of *absolute* inelastic cross sections for the CH–He system, if only at a single energy, would pose an additional stringent constraint on our ability to model theoretically rotational energy transfer in this system.

ACKNOWLEDGMENTS

M.H.A. and W.R.K. wish to acknowledge the support of the National Science Foundation under Grants No. CHE89-05912 and CHE92-23081 and the U. S. Army Research Office under Grant No. DAAL03-91-G-0129. A. E. W. is grateful for the support of the Office of Basic Energy Sciences, Division of Chemical Sciences, U.S. Department of Energy, under Contract No. W-31-109-Eng-38. The authors are grateful to Hans-Joachim Werner, Paul Dagdigian, Kopin Liu, and Glen Macdonald for their encouragement and for helpful discussions concerning collisions of Π-state molecules as well as the subtleties of the experiments reported in Refs. 18 and 19.

[1] K. Liu, R. G. Macdonald, and A. F. Wagner, Int. Rev. Phys. Chem. **9**, 187 (1990).
[2] M. H. Alexander, J. Chem. Phys. **76**, 5974 (1982).
[3] M. H. Alexander, Chem. Phys. **92**, 337 (1985).
[4] B. Pouilly and M. H. Alexander, J. Chem. Phys. **88**, 3581 (1988).
[5] R. Schinke and P. Andresen, J. Chem. Phys. **81**, 5644 (1984).
[6] D. P. Dewangan and D. R. Flower, J. Phys. B **18**, L137 (1985).
[7] D. P. Dewangan, D. R. Flower, and G. Danby, J. Phys. B **19**, L747 (1986).
[8] D. P. Dewangan, D. R. Flower, and M. H. Alexander, Mon. Not. R. Astron. Soc. **226**, 505 (1987).
[9] G. C. Corey and M. H. Alexander, J. Chem. Phys. **88**, 6931 (1988).
[10] A. Jörg, A. Degli-Esposti, and H.-J. Werner, J. Chem. Phys. **93**, 8757 (1990).
[11] A. Degli-Esposti and H.-J. Werner, J. Chem. Phys. **93**, 3351 (1990).
[12] T. Orlikowski and M. H. Alexander, J. Chem. Phys. **79**, 6006 (1983).

This article is copyrighted as indicated in the article. Reuse of AIP content is subject to the terms at: http://scitation.aip.org/termsconditions. Downloaded to IP: 141.209.100.60 On: Mon, 22 Dec 2014 16:43:09

[13] H. Joswig, P. Andresen, and R. Schinke, J. Chem. Phys. **85**, 1904 (1986).
[14] G. C. Corey and M. H. Alexander, J. Chem. Phys. **85**, 5652 (1986).
[15] H.-J. Werner, B. Follmeg, M. H. Alexander, and D. Lemoine, J. Chem. Phys. **91**, 5425 (1989).
[16] P. J. Dagdigian, M. H. Alexander, and K. Liu, J. Chem. Phys. **91**, 839 (1989).
[17] M. H. Alexander, P. Andresen, R. Bacis, R. Bersohn, F. J. Comes, P. J. Dagdigian, R. N. Dixon, R. W. Field, G. W. Flynn, K.-H. Gericke, B. J. Howard, J. R. Huber, D. S. King, J. L. Kinsey, K. Kleinermanns, A. C. Luntz, A. J. MacCaffery, B. Pouilly, H. Reisler, S. Rosenwaks, E. Rothe, M. Shapiro, J. P. Simons, R. Vasudev, J. R. Wiesenfeld, C. Wittig, and R. N. Zare, J. Chem. Phys. **89**, 1749 (1988).
[18] K. Liu and R. G. Macdonald, J. Chem. Phys. **89**, 4443 (1988).
[19] R. G. Macdonald and K. Liu, J. Chem. Phys. **91**, 821 (1989).
[20] R. G. Macdonald and K. Liu, J. Chem. Phys. **93**, 2431, 2443 (1989).
[21] A. F. Wagner, T. H. Dunning, Jr., and R. Kok, J. Chem. Phys. **100**, 1326 (1994).
[22] J. T. Hougen, Natl. Bur. Stand. (U.S.) Monogr. **115** (1970).
[23] R. N. Zare, A. L. Schmeltekopf, W. J. Harrop, and D. L. Albritton, J. Mol. Spectrosc. **46**, 37 (1973).
[24] H. Lefebvre-Brion and R. W. Field, *Perturbations in the Spectra of Diatomic Molecules* (Academic, New York, 1986).
[25] J. M. Brown, J. T. Hougen, K.-P. Huber, J. W. C. Johns, I. Kopp, H. Lefebvre-Brion, A. J. Merer, D. A. Ramsay, J. Rostas, and R. N. Zare, J. Mol. Spectrosc. **55**, 500 (1975).
[26] G. Herzberg, *Spectra of Diatomic Molecules*, 2nd ed. (Van Nostrand, Princeton, 1968).
[27] J. M. Brown and B. J. Howard, Mol. Phys. **31**, 1517 (1975); **32**, 1197 (1976).
[28] D. M. Brink and G. R. Satchler, *Angular Momentum*, 2nd ed. (Clarendon, Oxford, 1968).
[29] H. Klar, J. Phys. B **6**, 2139 (1973).
[30] D. Poppe, Chem. Phys. Lett. **19**, 63 (1973).
[31] S. Green and R. N. Zare, Chem. Phys. **7**, 62 (1975).
[32] A. Arthurs and A. Dalgarno, Proc. R. Soc. London, Ser. A **256**, 540 (1960).
[33] W. A. Lester Jr., Meth. Comp. Phys. **10**, 211 (1971).
[34] M. H. Alexander, P. J. Dagdigian, and D. Lemoine, J. Chem. Phys. **95**, 5036 (1991).
[35] K. P. Huber and G. Herzberg, *Molecular Spectra and Molecular Structure. IV. Constants of Diatomic Molecules* (Van Nostrand Reinhold, New York, 1979).
[36] HIBRIDON is a package of programs for the time-independent quantum treatment of inelastic collisions and photodissociation written by M. H. Alexander, D. E. Manolopoulos, H.-J. Werner, and B. Follmeg, with contributions by P. F. Vohralik, D. Lemoine, G. Corey, B. Johnson, T. Orlikowski, W. Kearney, A. Berning, A. Degli-Esposti, C. Rist, and P. Dagdigian.
[37] K. Liu (private communication, 1991).
[38] H. J. Korsch and R. Schinke, J. Chem. Phys. **75**, 3850 (1981).
[39] M. T. Berry, M. R. Brustein, M. I. Lester, C. Chakravarty, and D. C. Clary, Chem. Phys. Lett. **178**, 301 (1991).
[40] See, for example, S. Carter, N. C. Handy, P. Rosmus, and G. Chambaud, Mol. Phys. **71**, 605 (1990), and references contained therein.

This article is copyrighted as indicated in the article. Reuse of AIP content is subject to the terms at: http://scitation.aip.org/termsconditions. Downloaded to IP: 141.209.100.80 On: Mon, 22 Dec 2014 10:48:05